Available online at www.sciencedirect.com

ScienceDirect

Biomedical Journal

journal homepage: www.elsevier.com/locate/bj

Original Article

Evaluation of cell damage induced by irradiated Zinc-Phthalocyanine-gold dendrimeric nanoparticles in a breast cancer cell line

*Ivan Mfouo-Tynga, Nicolette Nadene Houreld, Heidi Abrahamse**

Laser Research Centre, Faculty of Health Sciences, University of Johannesburg, Johannesburg, Gauteng, South Africa

ARTICLE INFO

Article history:
Received 3 March 2017
Accepted 14 May 2018
Available online 6 September 2018

Keywords:
Cancer
Photodynamic effects
Nanomedicine
Cell damage
Cell death

ABSTRACT

Background: Cancer is a non-communicable disease that occurs following a mutation in the genes which control cell growth. Breast cancer is the most diagnosed cancer among South African women and a major cause of cancer-related deaths worldwide. Photodynamic therapy (PDT) is an alternative cancer therapy that uses photochemotherapeutic agents, known as photosensitizers. Drug-delivery nanoparticles are commonly used in nanomedicine to enhance drug-therapeutic efficiency. This study evaluated the photodynamic effects following treatment with 0.3 μM multiple particles delivery complex (MPDC) and irradiated with a laser fluence of 10 J/cm^2 using a 680 nm diode laser in a breast cancer cell line (MCF-7).

Methods: Cell damage was assessed by inverted light microscopy for cell morphology; the Apoptox-Glo triple assay was used for cell viability, caspase activity and identification of cytodamage markers; flow cytometric analysis for cell death pathways and mitochondrial membrane potential; the enzyme linked immunosorbent assay (ELISA) for cytochrome C release; and real-time reverse transcriptase polymerase chain reaction (RT-PCR) array for gene expression.

Results: Laser activated-MPDC induced a significant change in morphology of PDT-treated cells, with the appearance of apoptotic like morphological features. An increase in cytotoxicity, caspase activity, cell depolarization and cytochrome C release were identified in PDT-treated cells. Finally, the upregulation of BAX, BCL-2, CASP-2 and ULK-1 genes was observed.

Conclusion: The MPDC yielded a successful and stable hybrid agent with potent photodynamic abilities.

Cancer is a non-communicable disease that is characterized by abnormal cell proliferation and subsequent cellular damage. Cancer has become a major life threatening disease in both the developed and developing world, with more than 11 million projected deaths in 2030 [1,2]. In Africa, few resources are allocated to the fight against cancer and as a result the disease accounts for numerous deaths. Currently, cancer causes more deaths than tuberculosis, the acquired immune

* *Corresponding author*. Laser Research Centre, Faculty of Health Sciences, University of Johannesburg, P.O. Box 17011, Doornfontein, 2028, South Africa.
E-mail address: habrahamse@uj.ac.za (H. Abrahamse).
Peer review under responsibility of Chang Gung University.
https://doi.org/10.1016/j.bj.2018.05.002

At a glance commentary

Scientific background on the subject

Cancer is a major life threatening disease that requires vigorous treatment. Photodynamic therapy is an alternative therapy that uses photochemotherapeutic agents and low intensity laser irradiation to stimulate cell damage in the presence of molecular oxygen. This study investigated the effect of a multiple particle delivery complex in MCF7 cells.

What this study adds to the field

The novel multiple particle delivery complex (MPDC), consisting of sulfonated Zinc-Phthalocyanine and gold nanoparticle encapsulated dendrimers, yielded a successful and stable hybrid agent with potent photodynamic abilities. Conjugation could improve therapeutic outcomes to achieve better targeted therapy or better delivery to cancer cells, and increased cancer cell sensitivity to treatment.

deficiency syndrome (AIDS) and malaria combined [3,4]. Abnormal cell proliferation within the breast glands is known as breast cancer. This form of cancer is the most diagnosed cancer among South African women and a major cause of cancer-related deaths worldwide. Treatments for cancer have evolved from palliative to conventional therapies [3,5,6]. Photodynamic therapy (PDT) is an alternative cancer therapy that uses a photosensitizer (PS) and low intensity laser irradiation to stimulate cell damage in the presence of molecular oxygen [7]. The anticancer effects of PDT and the generation of reactive oxygen species (ROS) depends on the photophysical and photobiological abilities of the PS. Generated ROS can induce cell damage by various cell death mechanisms [8,9].

Research and development of new PSs is ongoing and crucial for the efficiency of PDT [10]. Nanotechnology is the engineering of small particles and is an interdisciplinary field set to revolutionize the fight against cancer by providing exceptional interaction of cancer cells with nanomaterials at both superficial and intracellular levels [11,12]. Nanoparticles (NPs) have been used in medical applications as imaging agents, therapeutic agents, diagnostic agents, active implants and drug-delivery agents [13]. NPs have attracted the attention of many researchers because of their high surface to mass ratio, quantum properties, and capacity to absorb and carry other compounds [14]. Drug-delivery NPs are commonly used in nanomedicine and offer additional benefits including the enhancement of drug-therapeutic efficiency and pharmacological properties by altering pharmacokinetics, improving drug hydro-solubility, drug half-life, bioavailability and target cell specificity [15]. This study looked at the mechanisms of breast cancer cell (MCF-7) damage mediated by a MPDC, which consisted of a sulfonated Zinc-Phthalocyanine mix ($ZnPcS_{mix}$) and gold nanoparticle encapsulated dendrimers (AuDENPs) [Fig. 1].

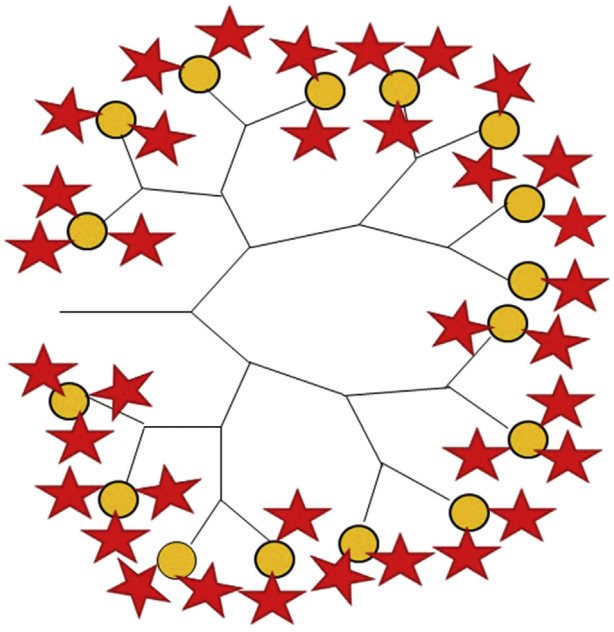

Fig. 1 Schematic representation of the MPDC, consisting of a gold-encapsulated dendrimer and 38 Sulfonated Zinc-Phthalocyanine mix.

Materials and methods

Cell culture and treatment

MCF-7 breast cancer cells (ATCC: HTB-22™, Lot Number: 60731981) were cultivated in Dulbecco's Modified Eagle Medium (DMEM, Gibco, 41966). The culture media was enriched with 10% fetal bovine serum (FBS, Gibco, 10106-169), 1% Amphotericin-B (Sigma, A2942) and 1% Penicillin-streptomycin (Sigma, P4333). Cells were incubated at 37 °C in 5% CO_2 and 85% humidity. Upon reaching confluency, cells were washed twice with Hank's Balance Salt Solution (HBSS, Gibco, 14065-056) before TryplE^{tm} Express (Gibco, 12604) was used to detach the cells from the culture flasks using 1 ml/25 cm^2. For experimental purposes, 5×10^5 MCF-7 cells (in 2 ml culture medium) were seeded in 3.4 cm diameter culture dishes and incubated for 4 h to allow the cells to attach. Fourth generation AuDENPs were mixed with $ZnPcS_{mix}$ at a ratio of 1:37.86 (v/v). The resultant particles is referred to as a multiple particles delivery complex (MPDC). Cells were treated with 0.3 μM MPDC and irradiated at a fluency of 10 J/cm^2 using a

Table 1 Laser parameters for irradiation.

Parameters	Diode laser
Manufacturer	Oriel Corporation
Wavelength	680 nm
Wave emission	Continuous
Spot size	9.1 cm^2
Output power	52 mW
Power density	5.73 mW/cm^2
Fluence	10 J/cm^2
Irradiation time	33 min 40 s

680 nm diode laser [Table 1]. Post-irradiation, the incubation periods of 3 and 24 h were considered for gene expression and biological assays, respectively.

Cell morphology

Morphological changes were examined in all control (no MPDC and no irradiation) and experimental groups 24 h post-irradiation. A CKX41 inverted light microscope (Olympus, Wirsam) connected to a camera was used to observe and capture qualitative changes with the analysis get IT software. Once digital images were captured, cells were detached and re-suspended for further biological analysis.

Biological assays

The ApoTox-Glo™ Triplex Assay (Promega, G6320) was performed to assess cell viability, cytotoxicity and caspase 3/7 activation and cleavage. A density of 2×10^5 cells per well was seeded and 20 μl of viability/cytotoxicity reagent was added, containing both glycyphenylalanyl-aminofluorocoumarin (GF-AFC) and bis-alanylalanyl-phenylalnyl-rhodamine 100 (AAF-R110) substrates for cell viability and cytotoxicity measurements respectively. Plates were placed on an orbital shaker (Heidolph Polymax Orbital, Labotec, 1040) set at 250 rpm for 1 min. Viable cells show a decrease in AFC fluorescence, while dead cells show an increase in R110 fluorescence. The mixture in a 96-well plate was incubated for 1 h at 37 °C before the fluorescence signals were recorded with $400_{Ex}/550_{Em}$ filters for viability and $485_{Ex}/535_{Em}$ filters for cytotoxicity. Thereafter, caspase 3/7 activity was measured by adding 100 μl of the Caspase-Glo 3/7 reagent to all wells and the luminescence signal was measured after 30 min of incubation at room temperature. All signal measurements were performed using the Victor^3 microplate reader (Perkin–Elmer).

Changes in mitochondrial membrane potential or depolarization of the mitochondrial transmembrane potential ($\Delta\Psi_m$) is associated with apoptosis, and the percentages of normal (polarized mitochondria) and damaged (depolarized mitochondria) cell populations were evaluated following treatment. Depolarized cells are unable to take up JC-1 stain and do not fluoresce in the red channel. Cells were detached as previously described, re-suspended in 1 ml HBSS and centrifuged at a speed of 400 × *g* for 5 min at a temperature of 4 °C. The supernatant was discarded and cells were re-suspended in 0.5 ml of a fresh JC-1 working solution (551302 Mitochondrial Membrane Potential Detection JC-1 kit, BD Biosciences) and thoroughly mixed. Then the mixture was incubated at 37 °C in a CO_2 incubator for 10 min, followed by the addition of 1 ml of 1 × assay buffer. The combination was mixed and centrifuged for 5 min at 400 × *g*. Again, the supernatant was discarded, 0.5 ml of 1 × assay buffer was added, the solution was vortexed and centrifuged in the same manner. Cells were re-suspended in 0.5 ml 1 × buffer and the cells in the pellet suspended by vortexing. Analysis was done using the FACSCAria flow cytometer (BD Biosciences).

Cytochrome C is an apoptogenic component required for further apoptotic events such as caspase-3 activation and DNA fragmentation. Mitochondrial damage and leakage were assessed with an enzyme linked immunoassay (eBioscience, BMS 263 human cytochrome C Platinum ELISA kit) to detect the level of cytosolic cytochrome C in various treated samples. Cells were detached from the plate, re-suspended in HBSS, centrifuged for 15 min at a speed of 217 × *g* and the supernatant was discarded. Thereafter, cells were re-suspended in 1 ml of cold phosphate buffer solution and centrifuged for 5 min at 398 × *g*. Cells were lysed by incubating with 0.5 ml of lysis buffer for 1 h at room temperature. Then, cells were centrifuged for 15 min at 217 × *g* and a 50-fold dilution of the supernatant was done by removing 5 μl of the supernatant and adding it into to a 1.5 ml tube with 245 μl of 1 × assay buffer. Samples (lysate supernatants) were further diluted by making a 1:2 dilution in assay buffer; 150 μl of sample was added to an equal volume of 1 × assay buffer, and a volume of 100 μl was added to the wells in a 96-well plate. Blank wells contained 100 μl of 1 × assay buffer added in duplicate, and all standards and samples were also added in duplicate. A volume of 50 μl biotin-conjugated anti-human cytochrome C antibody was added to all the wells and the microplate was covered with an adhesive film and incubated for 2 h at room temperature. Thereafter, the microplate was rinsed three times with 400 μl of wash buffer and 100 μl of Streptavidin-HRP secondary antibody was added to all the wells. The microplate was covered with an adhesive film and incubated for 1 h at room temperature. Then, the wells were washed three times with 400 μl of wash buffer, 100 μl of tetramethyl-benzidine (TMB) substrate was added and the plate was incubated at room temperature for 10 min. Lastly, the reaction was stopped by adding 100 μl of stop solution and the absorbance of each well was read at 450 nm using the Victor^3 microplate reader (Perkin–Elmer).

Cells were stained with Annexin V-fluorescein isothiocyanate (FITC) and Propidium iodide (PI) (BD Bioscience, 556547) to determine the mode of cell death. After treatment, cells were re-suspended, rinsed twice with PBS and then re-suspended in a 1 × assay binding buffer. A volume of 100 μl was transferred into a 15 ml Falcon™ tube and cells were concurrently incubated with 5 μl of Annexin V-FITC and PI. The mixtures were incubated in the dark for 5 min on ice. Then 400 μl of 1 × binding buffer was added to all the samples which were analyzed on the FACSCAria flow cytometer (BD Biosciences) by reading 10 000 events. Several control samples were included and prepared for the assay as follows: cells only without any stain; cells stained with Annexin V-FITC only; cells stained with PI only; and positive control cells which included those stained with both Annexin V-FITC and PI (late apoptotic). An apoptosis positive control was prepared by inducing apoptosis with 1 μg/ml actinomycin D, and a necrosis positive control with 10% (v/v) hydrogen peroxide for 24 h.

The real-time reverse transcriptase polymerase chain reaction (RT-PCR) was used to evaluate the expression of 84 genes following treatment (3 h incubation). Cells were detached and rinsed with PBS to remove all traces of culture media. Total RNA from untreated, MPDC-treated and PDT-treated cells was isolated using the RNeasy kit (Qiagen, 74104) with QIA shredder homogenizers (Qiagen, 79654). Cells were re-suspended in 600 μl RLT buffer and loaded on the QIA

cube (Invitrogen). At the end of the run, 30 μl of eluted RNA was collected and quantified using the Quant-iT™ RNA Assay kit (Invitrogen, Q32852) on the Qubit™ fluorometer (Invitrogen) according to the manufacturer's protocol. Two standards were used to calibrate the Qubit™ fluorometer and sample RNA concentration (μg/ml) was determined.

One microliter of sample RNA was mixed with 99 μl buffer AE (SABiosciences, 19077) in a quartz cuvette to determine RNA purity. The buffer consists of 10 mM Tris-Cl and 0.5 mM EDTA; pH 9.0. The absorbance of each sample was read using the Biomate 3 spectrophotometer (Thermospectronic, 335904P), and the ratio of the absorbance value at 206 nm over the value at 208 nm was calculated. All ratio values were between 1.82 and 2.01. Complementary DNA (cDNA) was reverse transcribed from 30 ng RNA using the QuantiTect Reverse Transcription kit, which included genomic DNA (gDNA) wipeout buffer. gDNA elimination was carried out for 8 min at 42 °C and the reaction stopped by placing the tubes on ice. Thereafter, a reverse transcription reaction with a final volume of 20 μl was prepared on ice by mixing Quantiscript Reverse Transcriptase, Quantiscript RT Buffer, RT Primer Mix and the gDNA elimination reaction (14 μl). The reverse transcription reaction tubes were vortexed and incubated for 15 min at 42 °C and then transferred and incubated for 3 min at 95 °C to deactivate Quantiscript Reverse Transcriptase. The purity of the cDNA samples was determined after obtaining the absorbance values and ratios (A260/280 nm) which were between 1.84 and 1.97. The real-time PCR array was performed and the synthesized cDNA used as a template.

The expression of 84 genes involved in death cell and senescence [Table 2] was analyzed using the Human Cell Death Pathway Finder™ PCR Array (SABiosciences, PAHS-212A) on the Stratagene Mx3000p. An additional 12 genes were integrated and consisted of 5 housekeeping genes (B2M, HPRT1, RPL13A, GAPDH, ACTB) to standardize the genes of interest, a gDNA control, positive PCR control genes (in triplicate) and a reverse transcriptase control gene (in triplicate). The cDNA samples were diluted to a final volume of 102 μl with RNase-DNase free water and used to prepare an experimental cocktail by adding the SABiosciences RT^2 qPCR master mix according to the manufacturer's protocol. The SABiosciences RT^2 qPCR Master mix used is designed for the Stratagene Mx3000p® and contains RT^2 SYBR Green (detected dye) and ROX (reference dye).

Twenty five microliters of the experimental cocktail was added to each well and the 96 well PCR Array plate was sealed with optical thin walled 8-cap strips and centrifuged for 1 min at room temperature at 1000 × *g* using a Heraeus Labofuge 400 centrifuge (Thermo Scientific) to remove all air bubbles. The run on the Stratagene Mx3000p® was programmed as follows: 1 cycle, 10 min at 95 °C to activate the HotStart DNA polymerase, and 40 cycles of 15 s and 1 min at 95 °C and 60 °C respectively (the annealing step).

The instrument software gave the threshold cycle (Ct) value for each well and all Ct values equal to or greater than 35 were considered as negative amplification (absence of amplicon). A gDNA control well (well H6) with a Ct value greater than 35 designated absence of gDNA contamination. Ct values of 20 ± 2 for positive PCR control wells should be obtained, which indicated successful amplification. The average Ct values of all 5 housekeeping genes was used by the software to normalize the 84 genes studied and was subtracted from the gene of interest Ct value. All Ct values were exported to a blank Excel spread sheet and used with the SABioscience PCR array Data Analysis Template available from the SABioscience website with the suitable pathway-focused genes (PAHS-212A). Fold-change ($2^{(\Delta\Delta Ct)}$) was calculated by the software by dividing the normalized gene expression ($2^{(\Delta Ct)}$) of the test sample by the normalized gene expression ($2^{(\Delta Ct)}$) of the control sample. Fold-change values greater than one indicate a positive or an up-regulation, and the fold-regulation is equal to the fold-change, while fold-change values less than one indicate a negative or down-regulation. The fold-regulation is the negative inverse of the fold-change.

Statistics

MCF-7 cells were taken from passage numbers 10–15. Results were averages of biochemical assays done in duplicate and repeated 4 times for cell damage analyses (n = 4). The one way ANOVA (one-tailed test) was done to compare treated cells to untreated cells, and statistical analysis was done using SigmaPlot Version 11.0 (Systat Software Incorporation). Graphs and tables depicted the obtained means and standard errors (±SEM) [16]. Statistical values were obtained at the 95th percentile and indicated as * for all $p < 0.05$, ** for all $p < 0.01$ and *** for all $p < 0.001$. Gene expression experiments were

Table 2 Functional gene grouping of the human cell death pathway finder profiler (updated from SABiosciences, PHAS-212A).

Cell death	Gene subunits
Pro-Apoptotic	ABL1, APAF1, BCL2L11, BIRC2 (c-IAP2), CASP1 (ICE), CASP2, CASP6, CASP7, CASP9, CD40 (TNFRSF5), CD40LG (TNFSF5), CFLAR (CASPER), DFFA, FASLG (TNFSF6), GADD45A, NOL3, TNFRSF10A (TRAIL-R).
Anti-Apoptotic	BCL2A1 (Bfl-1/A1), BIRC3 (c-IAP1), IGF1R, MCL1, TNFRSF11B, TRAF2, XIAP.
Apoptosis and Autophagy	AKT1, BAX, BCL2, BCL2L1 (BCL-X), CASP3, FAS (TNFRSF6), TNF, TP53.
Apoptosis and Necrosis	ATP6V1G2, CYLD, SPATA2, SYCP2, TNFRSF1A
Autophagy	APP, ATG12, ATG16L1, ATG3, ATG5, ATG7, BECN1, CTSB, CTSS, ESR1 (ERa), GAA, HTT, IFNG, IGF1, INS, IRGM, MAP1LC3A, MAPK8 (JNK1), NFKB1, PIK3C3 (VPS34), RPS6KB1, SNCA, SQSTM1, ULK1.
Necrosis	BMF, C1orf159, CCDC103, COMMD4, DEFB1, DENND4A, DPYSL4, EIF5B, FOXI1, GALNT5, GRB2, HSPBAP1, JPH3, KCNIP1, MAG, OR10J3, PARP1 (ADPRT1), PARP2, PVR, RAB25, S100A7A, TMEM57, TXNL4B.

repeated 3 times (n = 3) and the PCR Array data analysis software was utilized to determine the normalization, fold change (replicate $2^{(\Delta Ct)}$ values) and statistics. The p-value of fold change of individual gene in all samples was determined using the student's t-test.

Results

Cell morphology

Morphological features of MCF-7 cells were assessed following treatment with MPDC alone, laser irradiation alone and PDT (treated with MPDC and irradiated) [Fig. 2] and compared to untreated MCF-7 cells. Neither irradiated cells nor MPDC-treated cells showed detectable morphological changes. However, PDT-treated cells changed from a characteristic epithelial-like appearance and became irregular, with some cells rounding off and detaching from the culture flask and appearing as free floating structures.

Biological assays

The ApoTox-Glo™ Triplex Assay was performed to determine cellular viability, cytotoxicity, and caspase 3/7 activity, and results of treated cells were compared to those of untreated cells. Neither irradiation alone nor treatment with MPDC was able to induce a change in cell viability [Fig. 3], cytotoxicity [Fig. 4] and caspase activity [Fig. 5]. Thus, the MPDC alone as well as irradiation alone did not induce toxic effects. In combination with laser irradiation (10 J/cm^2), the MPDC induced marked changes including decreased viability ($p = 0.0008$), increased cytotoxicity ($p = 0.006$) and enhanced caspase activity ($p = 0.0007$). The MPDC had a photodamaging ability as it only showed a light-dependent toxicity.

Mitochondrial damage or destabilization was evaluated post-treatment in MCF-7 cells. The percentage of both polarized (black) and depolarized (gray) mitochondrial membrane potential in each treated cell group was determined and compared to the respective percentage of polarized or depolarized populations in the untreated control cells [Fig. 6]. After 24 h of incubation with the JC-1 fluorometric stain, no significant change in mitochondrial membrane potential (polarized and depolarized cells) was detected when cells were treated with irradiation alone or MPDC alone. However, a change in both the polarized and depolarized cell population was noticeable within PDT-treated cells. PDT-treated cells showed both an increase in the percentage of depolarized mitochondrial membrane and a decrease in the percentage of polarized membranes ($p = 0.008$). Thus, loss of mitochondrial membrane potential or damage was seen with light-activated MPDC.

The release of cytochrome C from the mitochondria is a critical event in cell damage. Cytochrome C levels in untreated and treated cells was determined by ELISA 24 h following

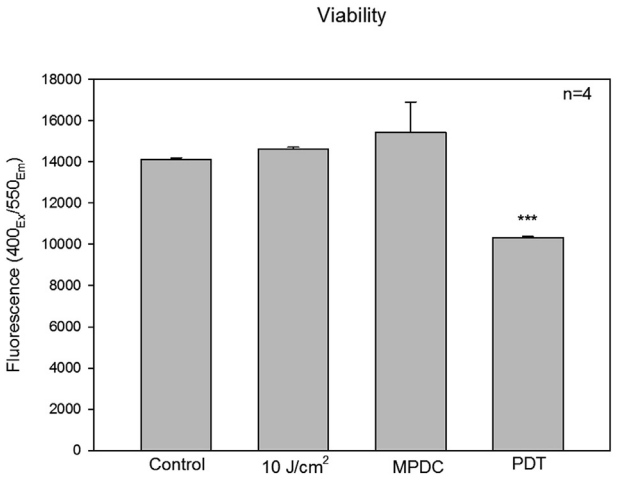

Fig. 3 ApoTox-Glo™ Triplex Assay Cell viability assay in MCF-7 cells using 400/550 ex/em filters. When compared to untreated control cells, the fluorescent signal of both laser irradiated and MPDC treated cells did not indicate any major change in cell viability. The irradiated MPDC exhibited a significant decrease in cell viability as *** ($p = 0.0008$).

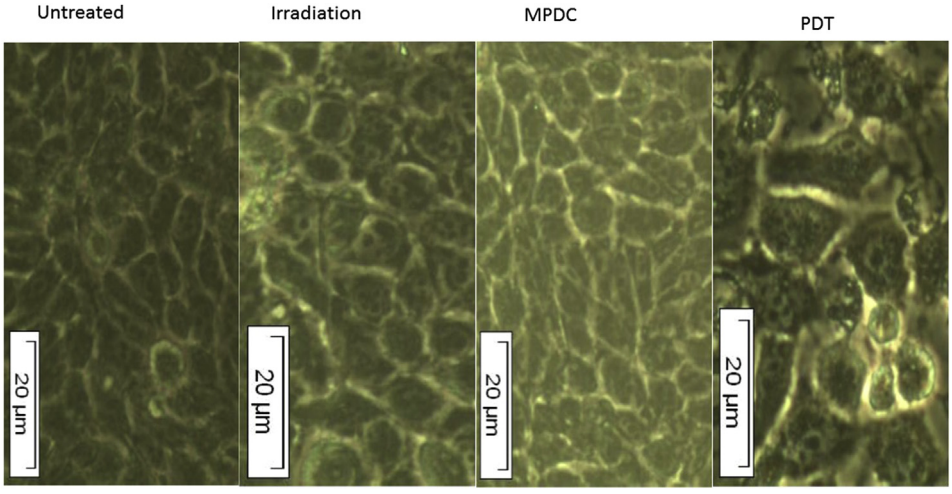

Fig. 2 Morphology of untreated, irradiated, MPDC-treated and PDT-treated MCF-7 cells. No morphological change was noted in irradiated or MPDC treated cells when compared to untreated cells. The morphology of PDT-treated MCF-7 cells changed, include an elongation of cells, decrease in cell number, detachment and rounding off (200× magnification).

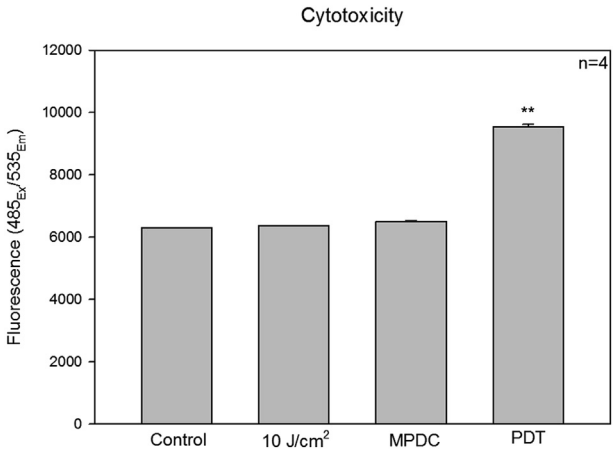

Fig. 4 ApoTox-Glo™ Triplex Cytotoxicity assay in MCF-7 cells using 485/535 ex/em filters. When compared to untreated control cells, the fluorescent signal of both laser-irradiated and MPDC-treated cells did not present any major increased toxicity. The irradiated MPDC exhibited an increase in cytotoxicity, shown as ** ($p = 0.006$).

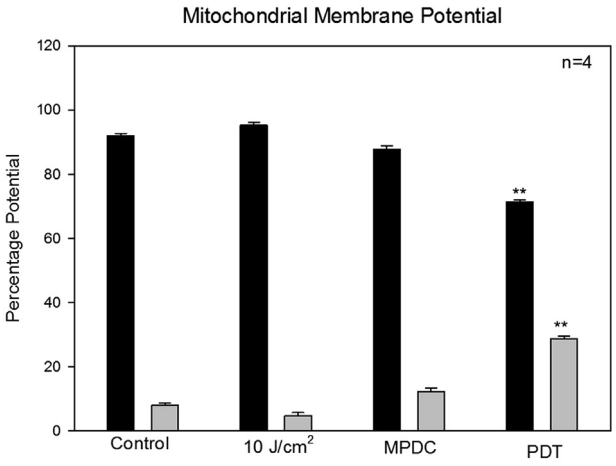

Fig. 6 Evaluation of mitochondrial membrane potential using flow cytometric analysis of JC-1 fluorometric stain. Percentage of polarized (black) and depolarized (gray) mitochondrial membrane potential were determined and compared to the percentage of the corresponding mitochondrial membrane potential of untreated, control cells. Only the PDT-treated cells showed a change in mitochondrial membrane potential ** ($p = 0.008$).

treatment. The results revealed that in the absence of laser irradiation the MPDC was unable to trigger an increase in the levels of cytochrome C [Fig. 7]. Laser irradiation alone was also not enough to lead to such an increase. MPDC coupled with laser irradiation was able to initiate cell damage and lead to an augmented level of cytochrome C ($p = 0.0005$).

Flow cytometric analysis using Annexin V-FITC and PI was performed to determine the foremost mode of cell death in MCF-7 cells following PDT with MPDC. Twenty four hours post-treatment, MCF-7 cells were stained and prepared for analysis. Additional controls were included in this experiment and consisted of MCF-7 cells treated with actinomycin D and hydrogen peroxide (H_2O_2) acting as apoptotic and necrotic controls, respectively. Different populations of cells were obtained: normal (negative for both Annexin V-FITC and PI), early apoptotic (positive for Annexin V-FITC and negative for PI), late apoptotic (positive for both Annexiv V-FITC and PI) and necrotic (positive for PI and made up of cells that were subjected to intensive damage). When cells were treated with actinomycin D or H_2O_2, significant changes ($p = 0.0004$ and 0.0007 for normal, $p = 0.0005$ and 0.03 for early apoptotic, $p = 0.0006$ for late apoptotic, and 0.02 and 0.0004 for necrotic cells) were seen with all cell populations when compared to their respective population type of the untreated control cells.

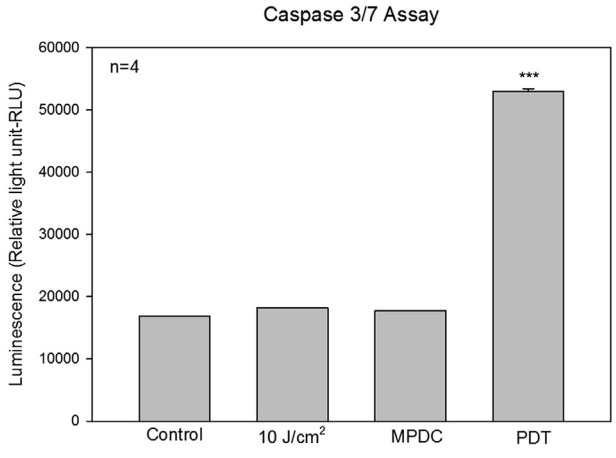

Fig. 5 ApoTox-Glo™ Triplex Assay Caspase luminescence assay in MCF-7 cells. When compared to untreated control cells, the luminescent signal of both laser-irradiated and MPDC-treated cells did not present any major increased caspase activity. The irradiated MPDC displayed a high luminescent signal, thus an enhanced caspase activity and is indicated as *** ($p = 0.0007$).

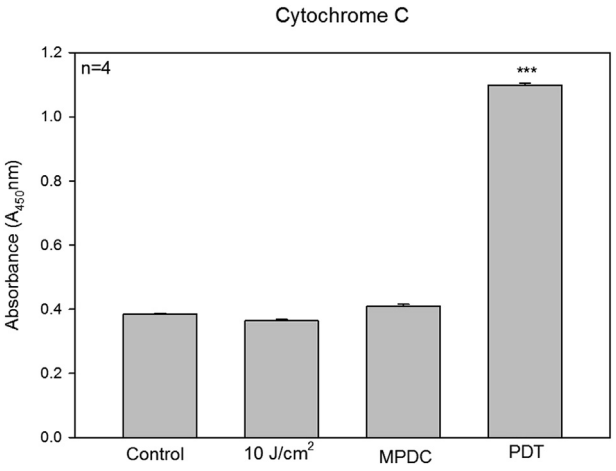

Fig. 7 Estimation of cytochrome C levels in untreated and treated MCF-7 cells. Cells treated with laser alone or MPDC alone did not lead to an increased colorometric signal when compared to the untreated cells. PDT-treated cells showed a significant increase shown as *** ($p = 0.0005$) and evidence of undergoing cell damage.

Table 3 Percentage of various cell populations following flow cytometric analysis. The lowest percentage of cell death (apoptotic and necrotic) and highest percentage of normal population were obtained with untreated cells. These apoptotic populations significantly increased (around 63%, accumulated percentage) in Actinomycin D-treated cells, and the highest percentage of necrotic population (42%) was seen with hydrogen peroxide (H_2O_2)-treated cells. Experiments were repeated four times (n = 4) and significant differences are indicated as *(p = 0.03 and 0.02) and * (p = 0.0007, 0.0006, 0.0006, 0.0005, 0.0004 and 0.0003) when compared to the respective population type of the untreated control cells.**

Cell populations	Untreated cells	Actinomycin D-treated cells	H_2O_2-treated cells
Normal	89 ± 2.05	26 ± 1.34***	9 ± 2.52***
Early apoptotic	7 ± 1.69	34 ± 0.49***	16 ± 2.62*
Late apoptotic	3 ± 2.65	29 ± 0.12***	33 ± 1.55***
Necrotic	1 ± 1.23	11 ± 1.63*	42 ± 1.02***

± represents standard error.

These treatments were able to induce cell death with apoptosis being more pronounced with treatment with actinomycin D as expected [Table 3]. Cells treated with laser irradiation alone or MPDC alone did not result in a significant change when compared to their respective population of untreated cells [Table 3]. However, PDT-treated cells showed significant changes with all populations ($p = 0.0006$ for normal, $p = 0.003$ for late and early apoptotic, and $p = 0.02$ for necrotic cells), with the apoptotic population being the most prominent (59% accumulated percentage) [Table 4].

Real-time RT-PCR was used to determine the regulation of 84 genes involved in cell death 3 h following treatment with 0.3 μM MPDC alone or with PDT. MCF-7 cells treated with 0.3 μM MPDC alone showed no significant up- or down-regulation of any genes as compared to the untreated control cells. The gene expression analysis of PDT-treated MCF-7 cells showed that BAX ($p = 0.035$), BCL2 ($p = 0.044$), CASP2 ($p = 0.006$) and ULK-1 ($p = 0.038$) were significantly up-regulated when compared to the untreated control cells [Fig. 8].

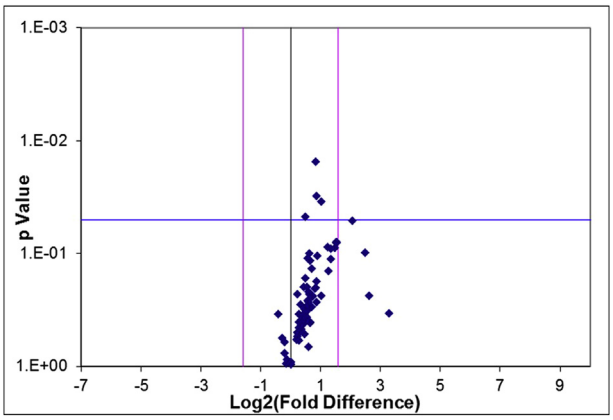

Fig. 8 Gene expression profiles of PDT-treated MCF-7 cells with 0.3 μM MPDC and 10 J/cm^2 was analyzed using the SABiosciences Human Cell Death Pathway Finder Profiler™ PCR Array System. PDT-induced changes in gene expression and BAX, BCL-2, CASP-2 and ULK-1 genes were significantly up-regulated as represented in the volcano plot. In the volcano plot, the horizontal line designates the target threshold ($p = 0.05$) and vertical lines, the fold change (central) and target fold change threshold (peripheral) in gene expression.

Discussion

Not only does various types of cancer cells react differently to different PSs, but cells also respond differently to diverse concentrations of PSs, wavelengths, power density and fluence of irradiation, and uptake of PSs. Previous work on the effects of PDT using $ZnPcS_{mix}$ on different cell lines has been conducted, and all results obtained were cell specific [7,17–27]. Hence, for each different type of cancer that is investigated, both PS concentration and laser irradiation fluence is determined in a dose response manner prior to conducting further investigation with respect to biological responsiveness of cells. The inverted light microscopic analysis was performed following treatment with both MPDC and laser irradiation in MCF-7 cells. Only laser-activated MPDC in the PDT-treated cells showed a significant change in cell morphology as compared to the untreated control cells. Some cells detached from the culture surface and appeared as free-floating structures, an indication of cell damage and confirming the ability of the MPDC to yield cytodamaging effects in MCF-7 cancer cells. Lee and co-workers (2009) confirmed cell morphological changes when conjugated AuNPs were used in lung cancer targeted therapy [28]. Another similar analysis was conducted and indicated that using AuNPs-

Table 4 Percentage of various cell populations following flow cytometric analysis. The lowest percentage of cell death (apoptotic and necrotic) were obtained with untreated and irradiated controls. These apoptotic populations significantly increased (around 65%) in MPDC- and PDT-treated cells. Experiments were repeated four times (n = 4) and significant differences are shown as *(p = 0.02), ** (p = 0.003) and * (p = 0.0006) when compared to the respective population type of the untreated control cells.**

Cell populations	Untreated cells	Irradiated cells	MPDC-treated cells	PDT-treated cells
Normal	89 ± 2.05	91 ± 1.11	86 ± 0.32	32 ± 1.06***
Early apoptotic	7 ± 1.69	6 ± 0.29	9 ± 2.12	29 ± 1.56**
Late apoptotic	3 ± 2.65	2 ± 2.45	4 ± 3.05	30 ± 1.74**
Necrotic	1 ± 1.23	1 ± 2.15	1 ± 1.84	9 ± 2.33*

± represents standard error.

targeted therapy in liver and lung cancer led to morphological changes and the appearance of apoptotic-like characteristic morphological features [29].

The ApoTox-Glo™ Triplex Assay was performed to determine cell viability, cytotoxicity and caspase 3/7 activity after treatment. It was revealed that light-activated MPDC prompted decreased cell viability and increased cytotoxicity and caspase 3/7 activity in MCF-7 cells. This showed that the MPDC in its active form following irradiation was able to induce significant damaging effects. Other studies have reported similar findings using various complexes containing AuNPs in different cancer cell lines. Decreased cell viability of breast, bladder and prostate cancer cells was seen following irradiation of drug-coated AuNPs for fibroblast growth factor 1 targeted cancer therapy [30]. Both 5 and 10 nm AuNPs containing compounds were endocytosed by A549 lung cancer cells leading to the inhibition of cell growth and increased cytotoxicity. These effects seemed to disappear when 20 and 40 nm sized compounds were utilized [31]. In another targeted therapy study, decreased viability, increased anti-proliferative and pro-apoptotic activity (such as increased caspase activity) were identified as the induced tumor suppressor response in breast cancer cells [32].

Results from this present study showed that mitochondrial integrity was not maintained after MPDC-mediated PDT in MCF-7 cells, as a change in the percentage of polarized and depolarized mitochondrial membrane potential was detected and indicated mitochondrial damage. A number of studies have reported that treatments using drugs, which localize in mitochondria, damage these cellular organelles triggering cell death through apoptotic pathways. Wen and co-workers (2013) reported that cancer treatment that targeted mitochondria led to dysfunctioning mitochondria with a shift in energy generation from oxidative phosphorylation to glycolysis, and noted high levels of ROS in various cell lines [33]. Treatment provoked a change in mitochondrial membrane potential, ROS levels and intracellular levels of ATP [34]. Pancratistin, an anti-cancer agent, triggered a decrease in mitochondrial membrane potential and led to the initiation of apoptosis in colorectal carcinoma cell lines [35].

NPs combined with therapeutic agents induced depolarization of the mitochondrial membrane potential, translocation of apoptosis inducing factor (AIF) and activation of caspase activity [36]. Rhodamine-^{123} accumulated in mitochondria and this accumulation lead to the disruption of mitochondrial membrane potential in kidney and breast cancer cells [37,38]. A similar disruption in mitochondrial membrane potential was seen with treatments using compounds such as RH1, edelfosine, doxobicin and curcumin as anti-cancer agents [39–42].

Mitochondrial damage has been linked to the release of cytochrome C. In this study, we used ELISA to determine the level of cytochrome C. It was found that the release of cytochrome C significantly increased after treatment with MPDC and laser irradiation in the PDT-treated cells. This concurs with work done by Heiligtag and associates (2002) when cerulenin, an anti-cancer agent, was able to damage mitochondria which led to the release of cytochrome C and the induction of apoptosis [43]. The induced release of cytochrome C is an important event for the activation of apoptotic cascades and caspase-dependent cell death [44,45]. The release of cytochrome C from the mitochondria was detected early and seemed to be critical for the initiation of cell death [46].

Annexin V-FITC and PI flow cytometric analysis established that apoptosis was the major induced cell death response after MPDC-mediated PDT in MCF-7 cells. The induction of apoptosis following mitochondrial damage was of no surprise as many previous studies confirmed the induction of apoptosis after treating cells with various mitochondrial damaging and anti-cancer agents in PDT [9]. PDT treatment that causes mitochondrial damage promotes apoptosis through the release of cytochrome C, AIF and other apoptogenic proteins such as caspases [47]. Hypericin-mediated PDT led to the initiation of apoptosis in a human hepatocellular liver carcinoma cell line (HepG2) after analyzing Annexin V-FITC/PI-stained cells using flow cytometry [48]. A large number of morphological changes including cell shrinkage, chromatin condensation, and nuclear fragmentation were detected and identified as typical apoptotic features in three cell lines (HeLa, HaCaT and MCF-7) when using cationic conjugated compounds containing ZnPC in PDT. And it was concluded that those cells had undergone apoptosis, which was detected 3 h after PDT [49].

Investigation into the expression of genes involved in cell death pathways was done 3 h following PDT to finally assess the efficacy of the conjugate in PDT and to determine which genes were primarily affected. It transpired that out of the 84 genes examined, 4 genes (BAX, BCL-2, CASP-2 and ULK-1) were significantly up-regulated in the PDT treated cells. Bax is an apoptosis regulator protein and member of the Bcl-2 family. It was among the first genes to be associated with pro-apoptotic activity. Its activation has been linked to the loss in mitochondrial membrane potential and the release of cytochrome C. Down-regulation or mutation of this protein leads to the suppression of apoptosis [50,51]. It exits as a cytosolic protein in normal cells, but upon induction of apoptotic signals it undergoes a conformational change and becomes associated with organelle membranes, in particular mitochondrial membranes [52]. Curcumin-induced up-regulation of BAX and cancer cell death through the mitochondrial-mediated apoptotic pathway [33].

BCL-2 encodes for another Bcl-2 family member protein that determines the commitment of cells to apoptosis [53]. Bcl-2 (B-cell lymphoma 2) regulates apoptosis by inducing or inhibiting apoptosis but it is principally considered as an anti-apoptotic effector and classified as an oncogene. In response to mitochondrial damage, release of cytochrome C, caspase activation and additional apoptotic events, BCL-2 is overexpressed to control those events [54].

Caspase 2 (CASP-2) is an apoptosis-related cysteine peptidase and involved in the initiation of apoptosis by participating in the formation of the CARD domain, RIP-associated Ich-1/Ced-3-homologue protein with a death domain (RAIDD), apoptosis repressor with caspase recruitment domain (ARC), and death effector filament-forming Ced-4-like apoptosis protein (DEFCAP). Nuclear damage is critically important for the expression of caspase-2 [55]. Additionally, caspase-2 can interact with the p53-induced protein with a death domain to form the PIPPosome, which is an activation platform for other

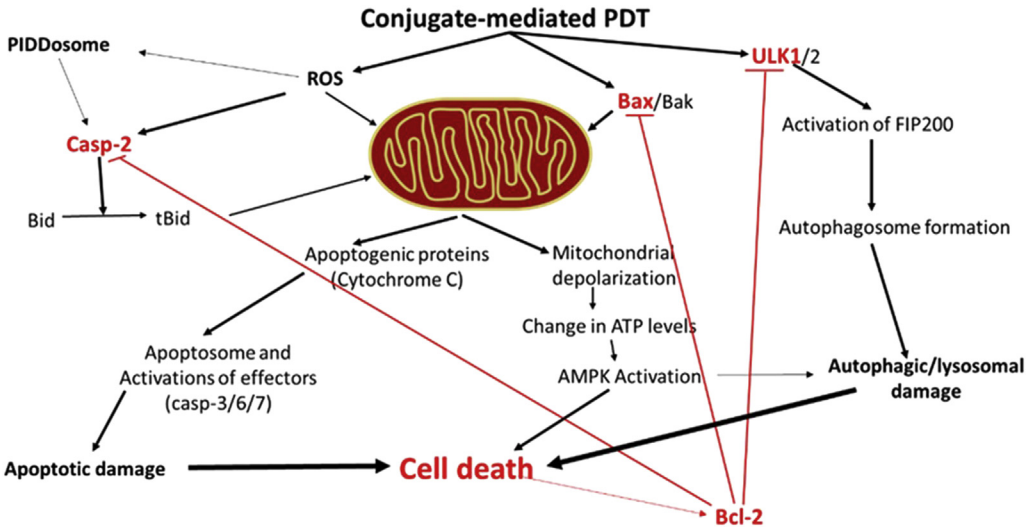

Fig. 9 The primary response of MPDC-mediated PDT on the expression of genes involved in cell death pathways was the up-regulation of Ulk-1, Bax, Casp-2 and Bcl-2 genes. The Ulk-1 protein protonates and activates the FIP200. ULK is part of a protein complex containing Atg13, Atg17 and FIP200 (autophagosome), which drives the subsequent cellular damage and death. The Bax protein directly affects the mitochondria while the Cas-2 protein is activated by reactive oxygen species (ROS) and then Casp-2 transforms a mitochondrial damaging protein into its truncated and activated form (tBid). The p53-induced death domain associated protein (PIDD) can also convert pro-Casp-2 into the active Casp-2. Apoptogenic proteins (such as Cytochrome C) released from mitochondria participate in the assemblage of the apoptosome, activation of other effectors (Casp-3/6/7) and cell death. Mitochondrial damage and depolarization induce change in cellular ATP levels, activation of the 5′ adenosine monophosphate activated protein kinase (AMPK) and AMPK-induced cell death. This cell death response stimulates Bcl-2 protein to prevent further cell damage.

proteases [56,57]. Robertson and colleagues (2002) found that caspase-2 additionally induces genetic damage and the induction of mitochondrial apoptotic pathway [46].

The fourth gene that was up-regulated, ULK-1 is associated with autophagy, which is both a survival and cell death mechanism. The ULK-1 gene is also known as the autophagy initiation kinase Unc-51-like kinase (ULK1)/ATG1. Ulk-1 is an autophagy initiator protein, which is indispensable for autophagic complex formation [58]. This complex consists of ulk-1, atg-13 and atg-17 and the complex leads to the formation of autophagosomes in the absence of mammalian target of rapamycin (mTOR) signal [59,60]. Autophagy has a cell death role and it was demonstrated that Ulk-1 also plays a role in ATP depletion and death in the presence of both PARP1 activity and H_2O_2 (vigorous damage). And the same study showed autophagy pro-death activity of Ulk-1 in response to ROS generation [61]. The schematic representation of the induced gene expression and cell death events of this present study is presented in Fig. 9.

Summary

The search for better and ideal PSs is indisputably encouraged. Combining AuDENPs and $ZnPcS_{mix}$ yielded a successful and stable hybrid agent with potent photodynamic abilities. The MPDC was able to induce subsequent cytodamaging effects. MCF-7 cells became sensitive to the treatment after PDT and the subsequent cellular damage included increased cytotoxicity, increased caspase activity, promotion of apoptotic-like events and upregulation of genes involved in apoptotic pathways. Conjugation could be considered as a way to improve the therapeutic outcomes of individual and less effective therapeutic agents to achieve better targeted therapy or better delivery to cancer cells, and increased cancer cell sensitivity to treatment.

The work presented in this paper is an in vitro study to determine the cellular response and mechanism of this new MPDC. Results presented here clearly indicate the therapeutic potential that this compound hold. However, to realize the clinical potential, *in vivo* and clinical trials will be performed in future.

Conflicts of interest

The authors declare we have no conflicts of interest.

Acknowledgements

The work was conducted at the Laser Research Centre, Faculty of Health Sciences, University of Johannesburg, South Africa. The study was supported by the University Research Council of the University of Johannesburg. This work is based on the research supported by the South African Research Chairs Initiative of the Department of Science and Technology and National Research Foundation of South Africa (Grant No

98337), and the African Laser Centre. We thank Mulisa S Nemanashi (Department of Chemistry, University of Johannesburg, South Africa) and Tebello Nyokong (Department of Chemistry, Rhodes University, South Africa) for their assistance with the synthesis of AuDENPs and $ZnPcS_{mix.}$ The National Laser Centre of the Council for Scientific and Industrial Research, South Africa is acknowledged for the supply and service of lasers.

Appendix A. Supplementary data

Supplementary data related to this article can be found at https://doi.org/10.1016/j.bj.2018.05.002.

REFERENCES

[1] Cannon G, Gupta P, Gomes F, Kerner J, Parra W, Weiderpass E, et al. Prevention of cancer and non-communicable diseases. Asian Pac J Cancer Prev 2012;13:3–11.
[2] Mozaffarian D, Fahimi S, Singh GM, Micha R, Khatibzadeh S, Engell RE, et al. Global burden of diseases nutrition and chronic diseases expert group. Global sodium consumption and death from cardiovascular causes. N Engl J Med 2014;371:624–34.
[3] Cancer Association of South Africa, South Africa. Prevalence cancer. 2016. http://www.cansa.org.za/south-african-cancer-statistics/ [Accessed 1 June 2016].
[4] Stefan DC, Elzawawy AM, Khaled HM, Ntaganda F, Asiimwe A, Addai BW, et al. Developing cancer control plans in Africa: examples from five countries. Lancet Oncol 2013;14:e189–95.
[5] American Cancer Society, USA. Cancer facts & figures 2014. Atlanta: American Cancer Society; 2015. http://www.cancer.org/ [Accessed 26 September 2015].
[6] Agostinis P, Berg K, Cengel KA, Foster TH, Girotti AW, Gollnick SO, et al. Photodynamic therapy of cancer: an update. CA Cancer J Clin 2011;61:250–81.
[7] Mfouo-Tynga I, Houreld NN, Abrahamse H. Induced cell death pathway post photodynamic therapy using a metallophthalocyanine photosensitizer in breast cancer cells. Photomed Laser Surg 2014;32:205–11.
[8] Mroz P, Yaroslavsky A, Kharkwal GB, Hamblin MR. Cell death pathways in photodynamic therapy of cancer. Cancers 2011;3:2516–39.
[9] Soriano J, Villanueva A, Stockert JC, Cañete M. Regulated necrosis in HeLa cells induced by ZnPc photodynamic treatment: a new nuclear morphology. Int J Mol Sci 2014;15:22772–85.
[10] Kessel D, Oleinick NL. Photodynamic therapy and cell death pathways. Methods Mol Biol 2010;635:35–46.
[11] Wei L. Nanoparticles for cancer treatment. Med Health RI 2012;95:249–95.
[12] Cai W, Chen X. Nanoplatforms for targeted molecular imaging in living subjects. Small 2007;3:1840–54.
[13] Selim ME, Hendi AA. Gold nanoparticles induces apoptosis in MCF-7 human breast cancer cells. Asian Pac J Cancer Prev 2012;13:1617–20.
[14] Lubick N, Betts K. Silver socks have cloudy lining. Environ Sci Technol 2008;42:e3910–6.
[15] Bednarski M, Dudek M, Knutelska J, Nowiński L, Sapa J, Zygmunt M, et al. The influence of the route of administration of gold nanoparticles on their tissue distribution and basic biochemical parameters: in vivo studies. Pharmacol Rep 2015;67:405–9.
[16] Cumming G, Fidler F, Vaux DL. Error bars in experimental biology. J Cell Biol 2007;177:7–11.
[17] Manoto S, Abrahamse H. Effect of a newly synthesized Zn sulfophthalocyanine derivative on cell morphology, viability, proliferation and cytotoxicity in a human lung cancer cell line (A549). Lasers Med Sci 2011;26:523–30.
[18] El-Hussein A, Abdel-Harith M, Abrahamse H. Assessment of DNA damage after photodynamic therapy using a metallophthalocyanine photosensitizer. Int J Photoenergy 2012;2012:281068.
[19] Horne TK, Abrahamse H, Cronje MJ. Investigating novel metallo-phthalocyanine PDT-induced MCF-7 cell death efficiency. Photodiagn Photodyn Ther 2012;9:215–24.
[20] Manoto S, Sekhejane P, Houreld NN, Abrahamse H. Localization and phototoxic effect of zinc sulfophthalocyanine photosensitizer in human colon (DLD-1) and lung (A549) carcinoma cells in vitro. Photodiagn Photodyn Ther 2012;9:52–9.
[21] Manoto SL, Houreld NN, Abrahamse H. Phototoxic effect of photodynamic therapy on lung cancer cells grown as a monolayer and three-dimensional multicellular spheroids. Lasers Surg Med 2013;45:186–94.
[22] Mfouo Tynga I, Houreld NN, Abrahamse H. The primary subcellular localization of Zinc Phthalocyanine and its cellular impact on viability, proliferation and structure of breast cancer cells (MCF-7). J Photochem Photobiol B: Biol 2013;120:171–6.
[23] Sekhejane P, Houreld N, Abrahamse H. Multi-organelle localization of metallated phthalocyanine photosensitizer in colorectal cancer cells (DLD-1 and CaCo-2) enhances efficacy of photodynamic therapy. Int J Photoenergy 2014;2014:383027.
[24] Mfouo Tynga I, El-Hussein A, Abdel-Harith M, Abrahamse H. Photodynamic ability of silver nanoparticles in inducing cytotoxic effects in breast and lung cancer cell lines. Int J Nanomed 2014;9:3771–80.
[25] El-Husseiny A, Mfouo Tynga I, Abdel-Harith M, Abrahamse H. Comparative study between the photodynamic ability of gold and silver nanoparticles in mediating cell death in breast and lung cancer cell lines. J Photochem Photobiol B 2015;153:67–75.
[26] Manoto S, Houreld NN, Abrahamse H. Resistance of lung cancer cells grown as multicellular tumour spheroids to zinc sulfophthalocyanine photosensitization. Int J Mol Sci 2015;16:10185–200.
[27] Mfouo Tynga I, Abrahamse H. Cell death pathways and phthalocyanine as an effective agent for photodynamic cancer therapy. Int J Mol Sci 2015;2015:10228–41.
[28] Lee CW, Chen MJ, Cheng JY, Wei PK. Morphological studies of living cells using gold nanoparticles and dark-field optical section microscopy. J Biomed Opt 2009;14:034016.
[29] Singh M, Kumar M, Manikandan S, Chandrasekaran N, Mukherjee A, Kumaraguru AK. Drug delivery System for controlled cancer therapy using physico-chemically stabilized bioconjugated gold nanoparticles synthesized from marine macroalgae, padina gymnospora. J Nanomed Nanotechol 2014;S5:009.
[30] Szlachcic A, Pala K, Zakrzewska M, Jakimowicz P, Wiedlocha A, Otlewski J. FGF1-gold nanoparticle conjugates targeting FGFR efficiently decrease cell viability upon NIR irradiation. Int J Nanomed 2012;7:5915–27.
[31] Liu Z, Wu Y, Guo Z, Liu Y, Shen W, Zhou P, et al. Effects of internalized gold nanoparticles with respect to cytotoxicity and invasion activity in lung cancer cells. PLoS ONE 2014;9:e99175.
[32] Selcuklu SD, Donoghue MT, Rehmet K, de Souza Gomes M, Fort A, Kovvuru P, et al. MicroRNA-9 inhibition of cell

proliferation and identification of novel miR-9 targets by transcriptome profiling in breast cancer cells. J Biol Chem 2012;287:e29516–28.
[33] Wen S, Zhu D, Huang P. Targeting cancer cell mitochondria as a therapeutic approach. Future Med Chem 2013;5:53–67.
[34] Le Bras M, Borgne-Sanchez A, Touat Z, El-Dein OS, Deniaud A, Maillier E, et al. Chemosensitization by knockdown of adenine nucleotide translocase-2. Cancer Res 2006;66:9143–52.
[35] Griffin C, Karnik A, McNulty J, Pandey S. Pancratistatin selectively targets cancer cell mitochondria and reduces growth of human colon tumor xenografts. Mol Cancer Ther 2011;10:57–68.
[36] Eloy L, Jarrousse AS, Teyssot ML, Gautier A, Morel L, Jolivalt C, et al. Anticancer activity of silver-N-heterocyclic carbine complexes. Caspase-independent induction of apoptosis via mitochondrial apoptosis-inducing factor (AIF). Chem Med Chem 2012;7:805–14.
[37] Summerhayes IC, Lampidis TJ, Bernal SD, Nadakavukaren JJ, Nadakavukaren KK, Shepherd EL, et al. Unusual retention of rhodamine 123 by mitochondria in muscle and carcinoma cells. Proc Natl Acad Sci USA 1982;79:5292–6.
[38] Bernal SD, Lampidis TJ, Summerhayes IC, Chen LB. Rhodamine-123 selectively reduces clonal growth of carcinoma cells in vitro. Science 1982;218:1117–9.
[39] Park MT, Song MJ, Oh ET, Lee H, Choi BH, Jeong SY, et al. The anti-tumour compound, RH1, causes mitochondria-mediated apoptosis by activating c-Jun N-terminal kinase. Br J Pharmacol 2011;163:567–85.
[40] Mollinedo F, Fernandez M, Hornillos V, Delgado J, Amat-Guerri F, Acuña AU, et al. Involvement of lipid rafts in the localization and dysfunction effect of the anti-tumor ether phospholipid edelfosine in mitochondria. Cell Death Dis 2011;2:e158–63.
[41] Kuznetsov AV, Margreiter R, Amberger A, Saks V, Grimm M. Changes in mitochondrial redox state, membrane potential and calcium precede mitochondrial dysfunction in doxorubicin-induced cell death. Biochim Biophys Acta 2011;1813:1144–52.
[42] Gogada R, Amadori M, Zhang H, Jones A, Verone A, Pitarresi J, et al. Curcumin induces Apaf-1-dependent, p21-mediated caspase activation and apoptosis. Cell Cycle 2011;10:4128–37.
[43] Heiligtag SJ, Bredehorst R, David KA. Key role of mitochondria in cerulenin-mediated apoptosis. Cell Death Differ 2002:1017–25.
[44] Gogada R, Prabhu V, Amadori M, Scott R, Hashmi S, Chandra D. Resveratrol induces p53-independent, X-linked inhibitor of apoptosis protein (XIAP)-mediated bax protein oligomerization on mitochondria to initiate cytochrome c release and caspase activation. J Biol Chem 2011;286:28749–60.
[45] Valero JG, Sancey L, Kucharczak J, Guillemin Y, Gimenez D, Prudent J, et al. Bax-derived membrane-active peptides act as potent and direct inducers of apoptosis in cancer cells. J Cell Sci 2011;124:556–64.
[46] Robertson JD, Enoksson M, Suomela M, Zhivotovsky B, Orrenius S. Caspase-2 acts upstream of mitochondria to promote cytochrome c release during Etoposide-induced apoptosis. J Biol Chem 2002;277:29803–9.
[47] Ribeiro JN, da SilvaI AD, Jorge RA. Involvement of mitochondria in apoptosis of cancer cells induced by photodynamic therapy. J Bras Patol Med Lab 2004;40:383–90.
[48] Barathan M, Mariappan V, Shankar EM, Abdullah BJJ, Goh KL, Vadivelu J. Hypericin-photodynamic therapy leads to interleukin-6 secretion by HepG2 cells and their apoptosis via recruitment of BH3 interacting-domain death agonist and caspases. Cell Death Dis 2013;4:e697–702.
[49] Acedo P, Stockert JC, Cañete M, Villanueva A. Two combined photosensitizers: a goal for more effective photodynamic therapy of cancer. Cell Death Discov 2014;5:e1122–8.
[50] Hassan M, Watari H, AbuAlmaaty A, Ohba Y, Sakuragi N. Apoptosis and molecular targeting therapy in cancer. BioMed Res Int 2014;2014:150845.
[51] Oltvai ZN, Milliman CL, Korsmeyer SJ. Bcl-2 heterodimerizes in vivo with a conserved homolog, Bax that accelerates programmed cell death. Cell 1993;74:609–19.
[52] Pierrat B, Simonen M, Cueto M, Mestan J, Ferrigno P, Heim J. SH3GLB, a new endophilin-related protein family featuring an SH3 domain. Genomics 2001;71:222–34.
[53] Czabotar PE, Lessene G, Strasser A, Adams JM. Control of apoptosis by the BCL-2 protein family: implications for physiology and therapy. Nat Rev Mol Cell Biol 2014;15:49–63.
[54] MacManus JP, Linnik MD. Gene expression induced by cerebral ischemia: an apoptotic perspective. J Cereb Blood Flow Metab 1997;17:815–32.
[55] Zhivotovsky B, Orrenius S. Caspase-2 function in response to DNA damage. Biochem Biophys Res Commun 2005;331:859–67.
[56] Manzl C, Krumschnabel G, Bock F, Sohm B, Labi V, Baumgartner F, et al. Caspase-2 activation in the absence of PIDDosome formation. J Cell Biol 2009;185:291–303.
[57] Tinel A, Tschopp J. The PIDDosome, a protein complex implicated in activation of caspase-2 in response to genotoxic stress. Science 2004;304:843–6.
[58] Alers S, Löffler AS, Wesselborg S, Stork B. Role of AMPK-mTOR-Ulk1/2 in the regulation of autophagy: cross talk, shortcuts, and feedbacks. Mol Cell Biol 2011;32:2–11.
[59] Mizushima N. The role of the Atg1/ULK1 complex in autophagy regulation. Curr Opin Cell Biol 2010;22:132–9.
[60] Jung CH, Jun CB, Ro SH, Kim YM, Otto NM, Cao J, et al. ULK-Atg13-FIP200 complexes mediate mTOR signaling to the autophagy machinery. Mol Biol Cell 2009;20:1992–2003.
[61] Joshi A, Iyengar R, Joo JH, Li-Harms XJ, Wright C, Marino R, et al. Nuclear ULK1 promotes cell death in response to oxidative stress through PARP1. Cell Death Diff 2016;23:216–30.